

THE EFFECT OF GRAVITY ON THE COMBUSTION SYNTHESIS OF Ni-Al AND Ni₃Al-TiB₂ COMPOSITES FROM ELEMENTS

Arvind Varma*, Hu Chun Yi, and Paul J. McGinn
University of Notre Dame
Notre Dame, IN 46556

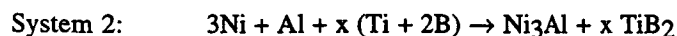
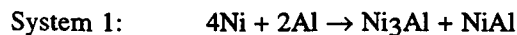
Introduction

Previous studies on the combustion synthesis of advanced materials indicate that combustion and structure formation mechanisms involve several stages including melting of reactants and products, spreading of the melt, droplet coalescence, diffusion and convection, buoyancy of solid particles, and densification of the liquid product. Most of these processes are affected by gravity. Conducting the combustion synthesis under microgravity conditions is expected to help elucidate the reaction mechanisms.

Although there have been a number of publications examining the role of gravity in materials processing [1-4], there is only limited work dealing with the effect of gravity on combustion synthesis. Hunter and Moore [5] recently compared the combustion synthesis of a number of ceramic-metal composites under both 1g and μ g conditions. While both the combustion temperature and wave velocity changed relatively little, they found that a more uniform microstructure resulted from the μ g condition.

Experiment

Two systems were examined. The first involves Ni/Al clad particles, which is an ideal system to examine the individual particle and liquid flow before combustion occurs. For comparison, elemental Ni and Al powders with the same stoichiometry as that of the clad particles were also used in some experiments. The reactant powders used in the present work are listed in Table I. Figure 1 shows a photomicrograph of the clad particles used in this investigation, which correspond to a composition of Ni(67.6 at%)-Al(32.3 at%). The second system was the Ni₃Al-TiB₂ composite in which the Ni₃Al ($-\Delta H_f^\circ = 153.1$ kJ/mol) phase melts during reaction enabling us to examine settling of the liquid phase. The amount of liquid phase was controlled by varying the TiB₂ ($-\Delta H_f^\circ = 323.8$ kJ/mol) content which generates the additional heat. The overall reactions for the two systems can be expressed as follows.



For the first system, pellets were pressed directly from the clad particles, at green densities about 77 \pm 3% of theoretical value. For the second, the pellets were prepared by mixing the elemental reactant powders in the required stoichiometry by ball-milling and then pressing uniaxially at green densities about 70 \pm 3% of theoretical. The pellets were cylindrical in shape, 10 mm in diameter and length typically 20-30 mm.

The pellet samples were reacted in UHP Argon (1 atm) using the experimental setup and procedure described previously [6]. After reaction, the samples were sectioned axially in order to conduct the microstructural analysis in the longitudinal direction. The phase composition of the reacted product was determined by X-ray diffraction (XRD) and the microstructure was analyzed using scanning electron microscopy (SEM) along with energy dispersive X-ray spectrometry (EDX).

* Author to whom correspondence should be addressed.

Results and Discussion

System 1: Ni/Al

Combustion of pellets pressed from cladded particles was extremely complex and exhibited features that have never been reported before. It was found that such pellets were more difficult to ignite than those pressed from elemental Ni and Al powders. Therefore, the section close to the ignition coil was always heated to a higher temperature than the remainder of the pellet before combustion started, which implies that the reaction was actually ignited from an elevated rather than room temperature. In fact, a pre-combustion wave, possibly corresponding to aluminum melting, was observed in many cases and the combustion started afterwards. Then a stable combustion occurred initially due to the preheating described above. When the combustion wave reached the less preheated part, it changed to an unstable and rather complex mode (combination of spin and oscillating, see also [7]). In some cases, the ignition either started from some distance away from the ignition coil, or started from the opposite end if the sample was short, and then propagated in a complex mode. In other cases, the combustion wave stopped during its progress. In yet other cases, the reaction started stable (preheating part) and propagated (unstable) downward to about 2/3 of the sample length and then stopped. Surprisingly, the reaction did not terminate at that point, but reinitiated from the opposite end after ~ 15 seconds and then propagated upward with a lower velocity. Visual observations revealed that the brightness of the reinitiated combustion was less as compared to the upper part. Examination of the sample after combustion showed that the lower part had a lower density. These facts indicate that the combustion temperature of the lower part was apparently lower.

The pellets were then combustion synthesized at elevated temperatures by preheating the green pellets using another W-coil placed around the pellet. For preheating temperatures over 200°C, the above described complex combustion did not occur. However, the combustion front was still quite irregular. Figure 2 shows the plots of combustion propagation velocity and combustion temperature (T_c) versus pre-heating temperature. It can be seen that the velocity increases only slightly with increase of preheating temperature above 200°C, while the combustion temperature shows a larger degree of variation.

The combustion of pellets from elemental Ni and Al powders does not have the complex features described above. When ignited at room temperature, the combustion wave propagates in a spin mode. Preheating above 200°C not only changes combustion to a stable one, but also increases the wave propagation velocity considerably, particularly above 300°C as shown in Fig. 2. This may be compared with results for cladded particles where relatively small velocity increment was observed. The same trend also holds for the combustion temperature, as shown in Fig. 2. Note that both the velocity and combustion temperature behave similarly in this case, indicating that a close relation exists between the two.

The product was examined by XRD and microscopy. It was found that the reacted product for both pellets, pressed from cladded particles or pressed from elemental Ni/Al powders, contained the same phases: NiAl, Ni₃Al and possibly Ni₅Al₃. An optical photomicrograph from a fully reacted part of a sample with cladded Ni/Al particles, is shown in Fig. 3. Figure 4 shows a SEM photomicrograph of the reaction front of a sample ignited at room temperature, which stopped in the middle of the pellet. At the reaction front, the NiAl phase formed between the cladded particles and indicates that the nickel shell broke up, molten aluminum flowed out, which then wet, spread, and reacted with nickel. This was also confirmed by in-situ observation of heating loose cladded particles using a high-speed video camera.

In the combustion synthesis of nickel aluminides from elemental powders, ignition and wave propagation usually result from melting and spreading of Al [8]. In these cases, once the Al melts, it immediately wets and spreads over the Ni, leading to product formation. However, for pellets pressed from cladded particles, the Ni shell reduces the wettability of liquid Al before it cracks, and the combustion rate is controlled by the outflow of liquid aluminum from inside the nickel shell. During heating up, the Al core melts first and liquid Al reacts immediately with solid nickel within the shell, forming NiAl₃ as observed by SEM and confirmed by EDX. However, this reaction is not responsible for the self-sustained combustion wave, which instead is caused by the outflow of Al from cracked Ni shell as stated above. Gravity may play a role in this process and future experiments conducted under microgravity will clarify this issue. Since the Ni shell reduces the wettability of molten Al, it is expected that the combustion rate for cladded particles is lower than that for elemental powders, leading to smaller propagation velocities as observed in Fig. 2.

System 2: Ni₃Al-TiB₂

Figure 5 shows the measured combustion temperature (along with theoretical adiabatic temperature) and wave velocity as a function of the amount of TiB₂ formed. Both combustion temperature and wave velocity increased dramatically with the TiB₂ content owing to the increased exothermicity of reaction. For samples containing more than 20 wt%TiB₂, the combustion temperature was higher than the melting point of Ni₃Al (1395 °C) so that a fully liquid phase was formed. For the 5 wt%TiB₂ sample, the combustion proceeded in an oscillatory and spin mode whereas for the 20 wt%TiB₂ sample, it propagated in a spin mode. For all samples with more than 40wt% TiB₂, a stable combustion was observed, although the wave front was not planar. It should be noted that the temperature measurement for samples containing more than 60 wt%TiB₂ was not accurate since the thermocouples (0.25 mm diameter, C-type) often broke during the combustion. However, Fig. 5 does show that the measured wave velocity had a trend similar to the adiabatic temperature. The combustion characteristics of the system are summarized in Table II, where the data are averages of two or more samples.

The XRD spectra showed complete reactions for all samples except the 5 wt% TiB₂, where traces of unreacted Ni and Al were also present. Figure 6 shows the morphology of the 40 wt% TiB₂ composite, indicating a relatively uniform distribution of the TiB₂ ceramic particles dispersed in the Ni₃Al matrix. Figure 7 shows some typical SEM photomicrographs of the same sample at different locations. It can be seen that the microstructure is non-homogenous. Apart from the uniform Ni₃Al-TiB₂ structure, there are also Ni₃Al islands of size 0.05-0.5 mm. Liquid settling clearly occurred at the bottom of the sample (Fig. 7c) and on the upper side of pores (Fig. 7b).

In order to further investigate the effect of gravity, the 40 wt% TiB₂ samples were also ignited from the bottom (placed vertically) and from the side (placed horizontally). While there was no substantial difference in the combustion temperature, the wave velocity was higher in both cases than when ignited from the top. Hunter and Moore [5] also observed similar results and attributed them to the preheating effect by the ignition coil. In the present work, the higher combustion velocity for the horizontal orientation was likely due to the fact that the pellet was placed in a semi-cylindrical quartz boat which may have decreased heat loss. The SEM examinations of the reacted products showed similar microstructure as in Figs. 6 and 7.

The terminal velocity of a spherical particle in a liquid medium under ideal conditions is described by the well-known Stoke's equation:

$$V_t = \frac{2}{9} \frac{g (\rho_s - \rho_l)}{\mu} R^2 \quad (1)$$

where g is the gravitational acceleration (9.81 ms^{-2} at 1 g and 9.81×10^{-3} at μg), ρ_s the density of the solid TiB₂ particle (4310 kgm^{-3}), ρ_l the density of the liquid Ni₃Al (6500 kgm^{-3}), and μ the dynamic viscosity (4.7×10^{-3} Pas). The last two properties were estimated from their elemental constituents assuming ideal mixing. Since the density of the liquid is larger than that of the solid particles, the liquid phase is expected to settle down. From the SEM photomicrographs shown in Fig. 6, the size of most TiB₂ particles ranges from 2-5 μm . Taking the average size as 3.5 μm , we have $V_t = 12.4 \mu\text{m/s}$. From the temperature profile recordings, the Ni₃Al phase stays in liquid state for 9.1 seconds for this particular sample. Hence, the settling of the liquid Ni₃Al phase should be about 113 μm . Measurements on different parts of the sample showed that the settling was between 10-30 μm . The measurements are comparable to the calculated values, especially given the numerous phenomena which would contribute to modifying eq. (1), including unsteady state, dynamics of particle formation, their non-spherical shape and large population. Under microgravity conditions, the settling effect would be greatly diminished (three orders of magnitude less).

Unstable convection may also play a role in this system. This phenomenon occurs when a fluid held in a container is heated from below, and the Rayleigh number defined as

$$Ra = \frac{\beta g \Delta T L^3 C_p \mu}{v^2 k} \quad (2)$$

exceeds a critical value which depends on the shape and dimensions of the container [4,9]. Here, ΔT is the temperature difference, L a characteristic length, β the liquid volumetric expansion coefficient, v the kinematic viscosity, C_p the specific heat and k is the thermal conductivity. Owing to complications of the geometry and the heterogeneous nature, it is difficult to evaluate the critical Rayleigh number for the present system. However, it is

clear that unstable convection is more likely to occur when the sample is ignited from the top, rather than from the bottom or the side. This issue is still under investigation. In any case, from eq. (2), it appears almost certain that unstable convection would not play a role under microgravity conditions.

Acknowledgement

This work was supported under NASA grant NAG3-1644.

References

1. Sharma S C, Narayanan P R, Sinha P P, Nagarajan K V, "Processing characteristics of Al/W composite under 1g conditions", *J. Mater. Sci.*, **29**, (1994), 5719-24 .
2. Froyen L, Deruyttere A, "Melting and solidification of metal matrix composites under microgravity", in 5th European Symposium on Material Sciences under Microgravity, Edited by Guyenne T D and Hunt, J J, Schloss Elmau, Germany (1984), 69-78.
3. Laxmanan V, Studer A, Wang L, Wallace J F, Winsa E A, "Gravitational macrosegregation in binary Pb-Sn alloy ingots", *Low-Gravity Sciences*, Edited by Koster J N, American Astronautical Society (1987), 119-48.
4. Ostrach S, "Convection phenomena of importance for materials processing in space", in *Materials Sciences in Space with Application to Space Processing*, Edited by Steg L, Progress in Astronautics and Aeronautics, **52**, (1977), 3-32.
5. Hunter K R and Moore J J, "The effect of microgravity on the combustion synthesis of ceramics and ceramic-metal composites", *J. Mater. Syn. Proc.* (in press).
6. Lebrat J -P, Varma A, and Miller A E, "Combustion synthesis of Ni₃Al and Ni₃Al-matrix composites", *Metall. Trans.* **23A**, (1992), 69-76.
7. Wenning L A, Lebrat J -P, and Varma A, "Some observations on unstable self-propagating high-temperature synthesis of nickel aluminides", *J. Mater. Syn. Proc.*, **2** (3), (1994), 125-32.
8. Lebrat J -P, Varma A, and McGinn P J, "Mechanistic studies in combustion synthesis of Ni₃Al and Ni₃Al-matrix composites", *J. Mater. Res.*, **2** (5), (1994), 1184-92.
9. Ostrach S, Pnueli D, "The thermal instability of completely confined fluids inside some particular configurations", *Trans. ASME, series C*, **85**, (1963), 346-54.

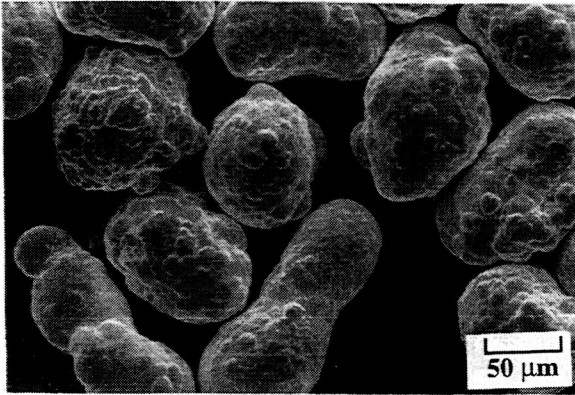
Table I. Characteristics of the Reactant Powders

Powder	Size, μm	Purity, %	Vendor
Ni	25 - 44	99.9	Cerac
Al	< 44	99.5	Aesar
Ti	< 44	99.5	Cerac
B (amorphous)			
Cladded Ni/Al	44 - 90	99.5	Sheritt Gordon
Ni	< 7	99.9	Aesar
Al	52 - 75	99.0	Aesar

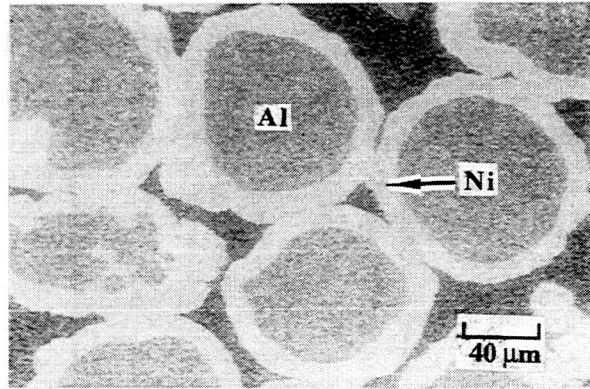
Table II. Combustion Characteristics of the Ni₃Al-xTiB₂ system

Composition (wt%TiB ₂)	T _c (°C)	Velocity (cm/s)	Propagation Mode
5	1351	-	Oscillatory
20	1384	1.2	Spin
40	1921 [†] 1932 1970*	3.6 [†] 3.2 4.1*	Stable
60	-	6.4	Stable
80	-	6.4	Stable

[†] Ignited from bottom. * Ignited horizontally.



(a)



(b)

Figure 1 - Cladded Ni-Al particles. (a) Morphology and (b) Cross-section.

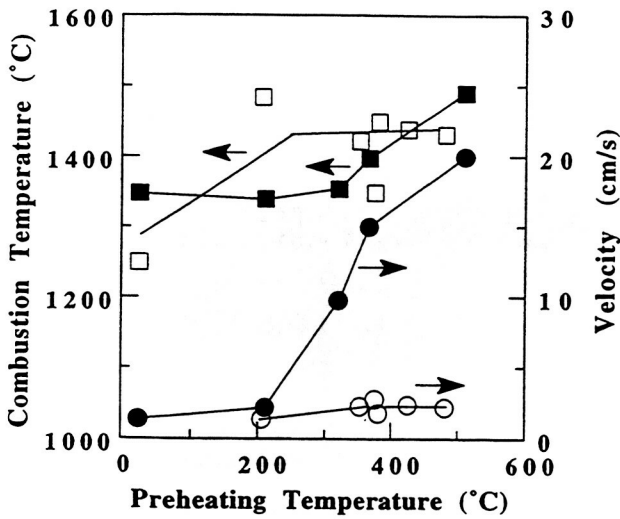


Figure 2 - Plot of combustion temperature and velocity versus preheating temperature for pellets from cladded (\square, \circ) and elemental (\blacksquare, \bullet) Ni/Al powders.

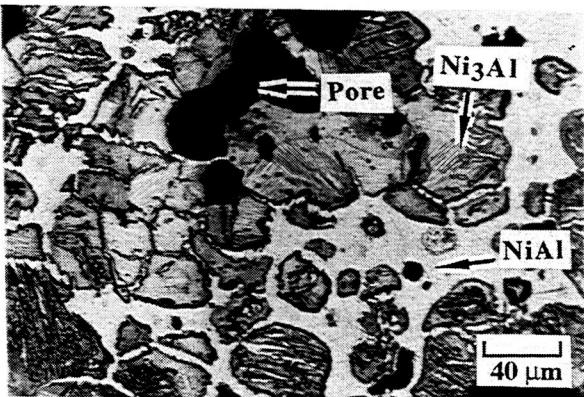


Figure 3 - Optical photomicrograph of the reacted pellet from cladded Ni/Al particles, showing the multiphase structure.

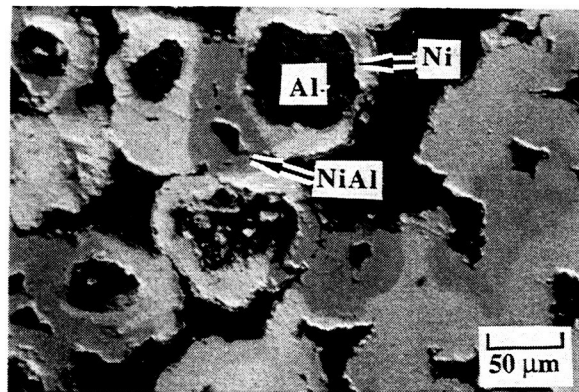


Figure 4 - Back-scattered SEM photomicrograph of reacted pellet from cladded Ni/Al particles, showing the reaction front.

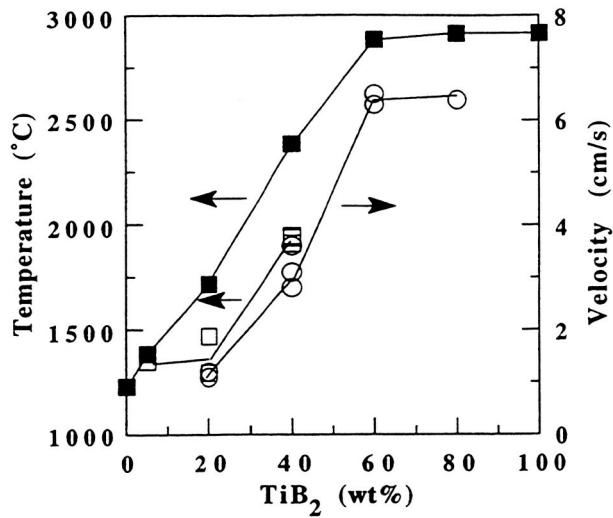


Figure 5 - Plot of measured combustion (□) and theoretical adiabatic (■) temperatures and velocity (○) versus TiB₂ amount.

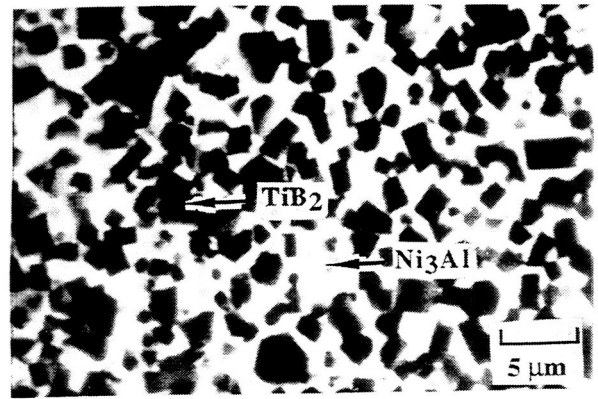
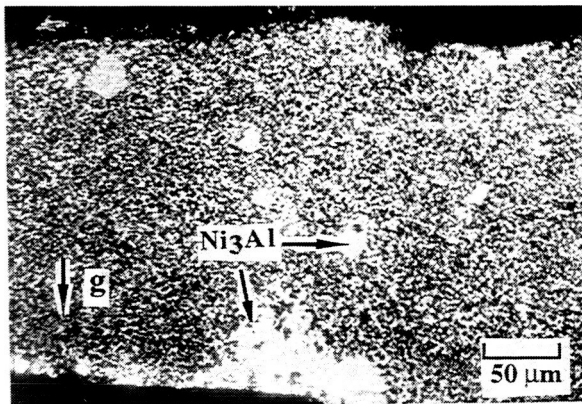
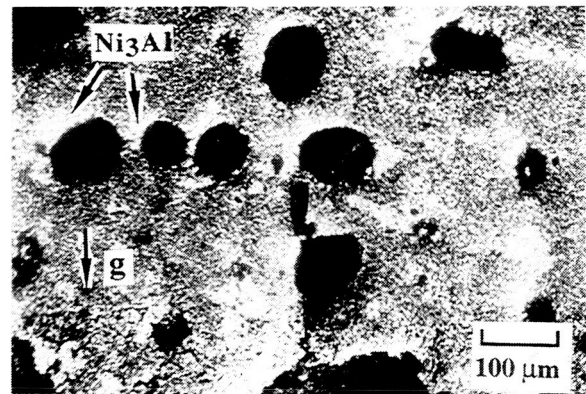


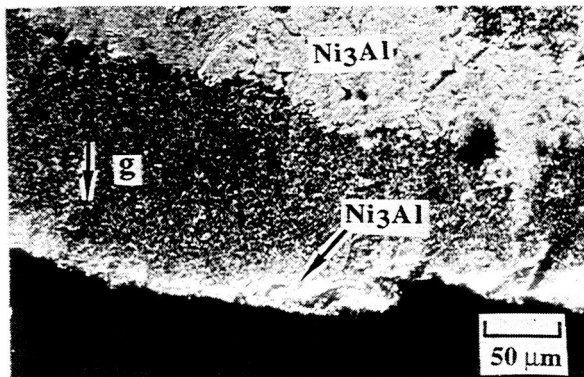
Figure 6 - Back-scattered SEM photomicrograph of a Ni₃Al-40wt% TiB₂ sample showing the size of TiB₂ particles.



(a)



(b)



(c)

Figure 7 - Back-scattered SEM photomicrographs of the same sample shown in Fig. 6, indicating settling of the Ni₃Al phase. (a) top part, (b) middle part, and (c) bottom part.